

GT2011-4), %

## EFFECT OF SCALING OF BLADE ROW SECTORS ON THE PREDICTION OF AERODYNAMIC FORCING IN A HIGHLY-LOADED TRANSONIC TURBINE STAGE

**Seyed Mohammad Hosseini**  
Royal Institute of Technology  
Heat and Power Technology  
S-100 44 Stockholm, Sweden

**Florian Fruth**  
Royal Institute of Technology  
Heat and Power Technology  
S-100 44 Stockholm, Sweden

**Damian M. Vogt**  
Royal Institute of Technology  
Heat and Power Technology  
S-100 44 Stockholm, Sweden

**Torsten H. Fransson**  
Royal Institute of Technology  
Heat and Power Technology  
S-100 44 Stockholm, Sweden

### ABSTRACT

The viability of a scaling technique in prediction of forced response of the stator and rotor blades in a turbine stage has been examined. Accordingly the so called parameter, *generalized force*, is defined which describes the excitation of a modeshape due to the unsteady flow forces at a certain frequency. The capability of this method to accurately predict the generalized forces serves as the viability criterion. The scaling technique modifies the geometry to obtain an integer stator, rotor blade count ratio in an annulus section while maintaining steady aerodynamic similarity. A non-scaled configuration is set up to serve as the reference case. Further configurations with different scaling ratios are also generated for accuracy comparison. Unsteady forces are calculated through 3D Navier-Stokes simulations by VolSol, which is based on an explicit, time-marching. A general purpose finite element model of blades is also provided to enable modal analysis with the harmonic forces. The generalized forces of stator and rotor blades revealed high sensitivity towards modification of stator blades while acceptable accuracy was obtained by moderate modifications of the rotor blades for first harmonic forces. Moreover the influence of variable blade's structural characteristics proved to be remarkable.

### 1. INTRODUCTION

As in many other fields turbomachine design requires numerous compromises among different aspects of design. With design progress, such compromises and revisions result in higher costs. Consequently the development of new

design tools which enable the prediction of certain design parameters at the very early stages of design has attracted growing attention in the last decades. One such area of research is the *aeroelastic* behavior of blades in a turbomachine namely, *Flutter*, and *HCF (High Cycle Fatigue)*. The latter is mostly referred to as structural fatigue of an entity subjected to continuous oscillatory motion. The intense flow-structure interactions and the cyclic nature of HP turbomachine stages make its occurrences eminent which is the focus of this study.

Formerly, according to the complexity of the problem, detecting its behavior and stresses could not be determined until the very last stages of design, causing extensive revisions and high costs. With the advancement of computational resources over the last decades, further studies are focused on development of methods which are capable of routine application with minimum computational cost, and time, accompanied by adequate accuracy.

A number of studies have targeted determination of appropriate parameters for forced response analysis. Studies by Jöcker. [1] showed that mode excitability can be used to determine risky operation points. Vahdati et al. [2] argued the unsteady pressure and structural modeshapes to be major players in risk assessment of oscillations. Moreover Mårtensson et al. [3] used a new method which assumes the modal forces to be proportional to the tangential forces known from operation charts. Having the modal forces, along with damping enables the finite element models to predict the present resonances in the operating range. Further analysis focused on efficient methods to extract

such parameters. Studies from Erdos et al. [4] address the periodicity of flow through development of *Chorochronic Periodicity*. In this technique the flow solution is stored in the pitch wise boundaries to be used as the boundary condition for the successive period. One drawback of such methods lies in their incapability to capture non-linear flow effects with the assumption of time periodicity i.e., 3D vortices. Moreover Giles et al. [5] developed the *Time Inclination Method* which does not assume time periodicity, also used by Laumert et al. [6]. In this technique the governing equations are transformed to serve the time inclination purpose. The method has its own weakness when it comes to certain blade count ratios when it faces instability.

The aforementioned mainly tackle the numerical algorithms. Further studies have directed their attention towards computational domain reduction by partial annulus simulations. Studies from Clark et al. [7], Schmitz et al. [8], Mayorca et al. [9] investigated the effect of the blade row interactions via the so called *Scaling Technique*. It combines the use of periodic boundary conditions with geometrical modifications. Periodic boundary condition not always allows partial annulus simulation towards any arbitrary blade count ratios. The scaling technique copes with the challenge through geometrical modification, enabling any arbitrary blade count ratios. This establishment of spatial periodicity allows for the application of any numerical flow solver. Hence the capability of this method in capturing complex flow features depends on the flow solver and its handling of time and space periodicity. This method has remarkable performance in computational domain reduction compared to the aforementioned methods.

The reported results from Schmitz et al. [8] in a turbine stage show good accuracy in prediction of generalized forces. Same condition persists for results from a fan stage, studied by Mayorca et al [9]. In contrast, results from Clark et al. [7] show high discrepancies in unsteady pressure among any slightly scaled cases making them incompetent for routine applications.

This study focuses on the forced response behavior of a turbine stage by employing the scaling technique. The accuracy of the predicted generalized forces serves as the viability of this method. Detailed analysis is also performed to determine the flow features influence by geometrical modification.

## 2. NOMENCLATURE

### Symbols

$dx, dy, dz$	Modal displacement [m]
$F$	Force [N]
$\bar{F}_t$	Mean tangential force [N]
$k$	Turbulent kinetic energy
Rad	Radial coordinates [m]

$S_r$	Rotor scaling ratio
$S_s$	Stator scaling ratio
$T$	Period of excitations [s]
$T_{in}$	Inlet static temperature
$P$	Pressure [Pa]
$P_0$	Total pressure [Pa]
$\tilde{p}$	Normalized unsteady pressure
$\bar{p}$	Mean pressure
$\epsilon$	Turbulent dissipation
$\theta$	Blade row sector angle [rad]
$\omega$	Rotational speed [rpm]

### Subscripts

cos	Real component (cosine)
gen	Generalized
i	Number of sampling time
j	Number of harmonics
norm	Normalized
sin	Imaginary component (sine)

## 3. METHOD

Scaling is basically a technique in which the geometry is slightly modified from the original geometry in order to establish spatial periodicity, in other words such a technique allows for any arbitrary integer blade count ratios between two adjacent blade rows. A sensitivity analysis is henceforth performed to study the effect of such modification on the forced response prediction.

The 3D in-house Navier-Stokes solver VolSol developed by Volvo Aero Corporation has been used in order to extract the unsteady aerodynamic forces acting on the blades. It is based on an explicit, time-marching, cell centered finite volume method. The time integration is handled with an explicit three-stage Runge-Kutta procedure, providing second order accuracy in time. For turbulent flow modeling a two equation k- $\epsilon$  model with standard wall functions is applied. The convective and viscous fluxes are calculated with a third order upwind scheme and a second order centered scheme.

The forced response analysis are performed in the frequency domain, therefore the unsteady forces from CFD simulations are Fourier transformed and back-scaled to be projected onto the modeshapes obtained from the structural model. The results are the generalized forces for each modeshape of the structure which are later normalized by the mean tangential force of the original machine. The generalized forces are then compared to measure the error margin relevant to the scaling ratio.

### 3.1. SCALING TECHNIQUE

The modifications are performed while minimizing their effect on steady aerodynamics. The conditions for such an assumption are threefold: maintaining solidity, thickness angles, as well as the channel inlet and outlet diameter along the blades (see Ref. [9]).

An overall scaling ratio needs to be defined to represent the level of geometrical modification (equation 1-3). This ratio can be defined on the basis of blade count ratios of the original and scaled machine for each individual blade row (equation 4-7).

$$S_r = \frac{\# \text{ of Original Rotor Blades}}{\# \text{ of Scaled Rotor Blades}} \quad (1)$$

$$S_s = \frac{\# \text{ of Original Stator Blades}}{\# \text{ of Scaled Stator Blades}} \quad (2)$$

$$S_{\text{overall}} = \frac{S_r}{S_s} \quad (3)$$

Once the number of blade rows of the intended scaled machine is determined, blades can be scaled along the axial and circumferential coordinates respectively (equation 4-7).

$$Rad = \text{Sqrt}(Z \cdot Z + Y \cdot Y) \quad (4)$$

$$X_{\text{scaled}} = X \cdot S_{\text{overall}} \quad (5)$$

$$Y_{\text{scaled}} = Rad \times \cos(S_{\text{overall}} \cdot \theta) \quad (6)$$

$$Z_{\text{scaled}} = Rad \times \sin(S_{\text{overall}} \cdot \theta) \quad (7)$$

The unsteady calculations are then performed incorporating the scaled geometry.

### 3.2. POST-PROCESSING

The extracted forces from the scaled machine mainly differ in amplitude, and frequency; therefore adjustments must be made to enable a viable comparison between the two machines in the temporal domain. As such the unsteady forces are Fourier transformed and back-scaled proportional to the scaling ratios (equation 8).

$$F_{\text{cos},j} = \frac{2}{N} \sum_{i=1}^N \frac{F_i}{S_r \cdot S_s} \cdot \cos\left(\frac{2 \cdot j \cdot \omega \cdot t_i}{T}\right) \quad (8)$$

$$F_{\text{sin},j} = \frac{2}{N} \sum_{i=1}^N \frac{F_i}{S_r \cdot S_s} \cdot \sin\left(\frac{2 \cdot j \cdot \omega \cdot t_i}{T}\right)$$

Two types of forces mostly contribute to the motion of a blade, external and motion induced forces. The latter is not the focus of this study and merely the mode excitability by external harmonic forces are studied. The dot product of the eigenvectors of an arbitrary structural modeshape and the vector from the external harmonic forces, normalized by the maximum oscillation amplitudes gives the value of generalized forces. In order to compare these values between different machines they are normalized by the mean tangential force of the original machine (equation 9-11).

$$F_{\text{gen},\text{cos},j} = \frac{\sum_{n=1}^N (F_{x,\text{cos},j,n} dx_n + F_{y,\text{cos},j,n} dy_n + F_{z,\text{cos},j,n} dz_n)}{A_{\text{max}}} \quad (9)$$

$$F_{\text{gen},\text{sin},j} = \frac{\sum_{n=1}^N (F_{x,\text{sin},j,n} dx_n + F_{y,\text{sin},j,n} dy_n + F_{z,\text{sin},j,n} dz_n)}{A_{\text{max}}}$$

$$F_{\text{gen}} = \sqrt{F_{\text{gen},\text{cos}}^2 + F_{\text{gen},\text{sin}}^2} \quad (10)$$

$$F_{\text{gen},\text{norm}} = \frac{F_{\text{gen}}}{\bar{F}_t} \quad (11)$$

## 4. TEST CASES

In this study, the BRITE EURAM transonic high pressure turbine stage MT1 has been used. It has been under a measurement campaign at DERA, Pyestock. The operating conditions are reported by Hilditch et al. [10, 11]. Figure 4-1 shows the profile of the stage, the blunt air sections and twisted rotor blades are some of the main characteristics of the turbine. The original geometry has the blade count ratio of 32:60. The current computational domain can be reduced to a blade count ratio of 8:15 without the need of scaling technique implementation; however as previously mentioned, this is not usually the case in most machines. The S8R15 case is to serve as the non-scaled case for sensitivity analysis.

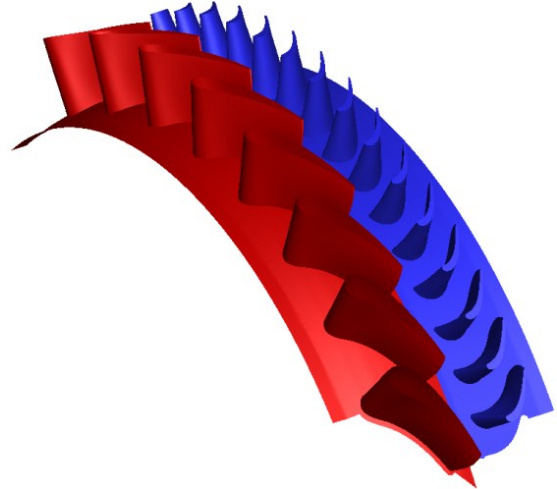


Figure 4-1: Non-scaled stage S8R15

Further scaled cases are selected with different overall scaling ratios, which cover a fraction of the full annulus. Table 4-1 shows such cases and the computational domain reduction they provide. The six different cases cover both negative and positive overall scaling ratios. As it will be illustrated later the negative and positive values have strong influence on the accuracy of the predicted generalized forces. S3R5, S4R7, S5R9 are positively scaled cases. In other words in such cases the stator blades are subjected to more size modification with respect to the rotor blades. The minimum absolute scaling ratio is achieved by S5R9, while S3R7 has the maximum absolute scaling ratio. It can be

observed that the overall scaling technique and its ability to reduce the computation domain strongly depends on the original blade count ratio of adjacent blades rows. It must be noted that the selection of S2R4 was due to the handling of the specific tool used to have multiple passages as an alternative to its identical S1R2 case.

**Table 4-1. Scaled configurations for numerical simulations**

Case	S8R15	S2R4	S3R7	S3R5	S4R7	S5R9	S6R13
Stator blades in Sector	32	2	3	3	4	5	6
Stator blades in 360	32	30	30	36	36	35	30
$S_s$	1	1.06	1.06	0.88	0.88	0.91	1.06
Rotor blades in Sector	60	4	7	5	7	9	13
Rotor blades in 360	60	60	70	60	63	63	65
$S_r$	1	1	0.86	1	0.95	0.95	0.92
$S_{overall}$	1	0.94	0.80	1.125	1.07	1.04	0.87
$S_{overall}$ (%)	0	-6.2	-19.6	12.5	7.1	4	-13
# Nodes (mil)	2,1	0.5	0.9	0.7	1.1	1.3	1.7
Time Step(s)	1e-7	1e-7	9e-8	1e-7	1e-7	8e-8	9.7e-8

#### 4.1. MESH

Figure 4-2 illustrates the current 3D structured mesh generated by the in-house software G3DMESH developed by Volvo Aero Corporation. An O-grid has been generated around the blade sections to achieve the required wall resolution. The boundary layer is resolved with  $y^+$  values varying from 20 to 200. One passage consists of 12 separate blocks to control the mesh diffusion with a provision for tip clearance of the rotor blade.

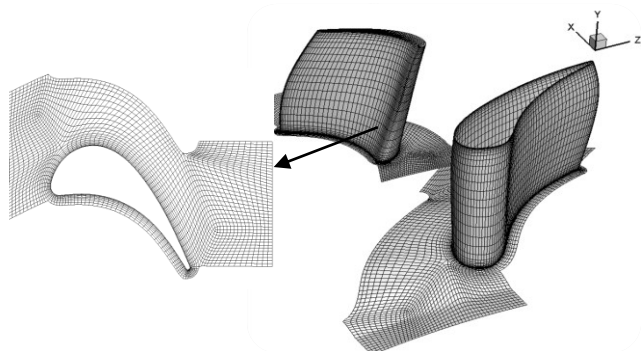


**Figure 4-2: 3D Structure mesh for numerical flow simulation**

#### 4.2. STRUCTURAL MODEL

Two FEM models are developed for stator and rotor blades with exclusion of the disk. Ansys Solid 45 elements are employed with a fully structured mesh to extract the modeshapes and their attributing natural frequencies. The stator blade is entirely clamped at hub and tip, while rotor is restrained at the hub. Grid independency of modeshape was established with a high quality mesh. Figure 4-3 shows the FEM model for the stator and rotor blade.

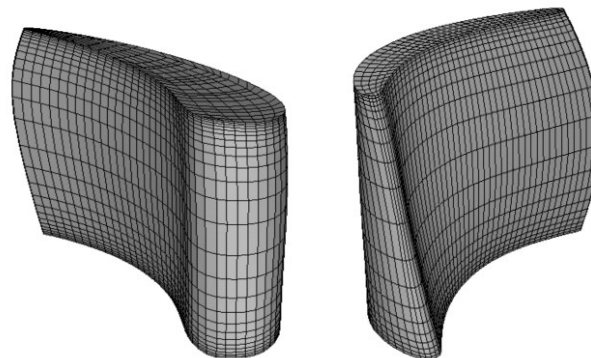


**Figure 4-3: FEM mesh of the stator blade (left) and the rotor blade (right)**

#### 5. RESULTS

The following section presents the steady and unsteady simulation results in addition to the calculated generalized forces. A discussion section is also included to point out the nature of excitation sources and their contributing effects.

##### 5.1. STEADY SIMULATIONS

Steady simulations are necessary to check the flow regime under the boundary conditions of Table 5-2. They can further be used as an initial solution to the unsteady simulation prompting quicker convergence. The applied boundary conditions are set for a pressure ratio of 0.31.

**Table 5-2. Boundary Conditions**

Boundary Conditions	Inlet	Outlet
$T_{in}$	444.4 K	412 K
$P_0$	461500 Pa	142500 Pa
$k$	70	298
$\epsilon$	47000	4,580,000
$\omega$	9500rpm	

Figure 5-1 shows the steady flow regime under transonic boundary conditions. Strong shock waves can be observed on the suction side of the stator blades particularly near the hub. A velocity deficient region is noticeable at the trailing edge emanated from the generated wakes. The shock and wake interactions are apparent near the trailing edge.

Further shockwaves can also be observed on the rotor's trailing edge which generally depicts a predominant transonic flow regime.

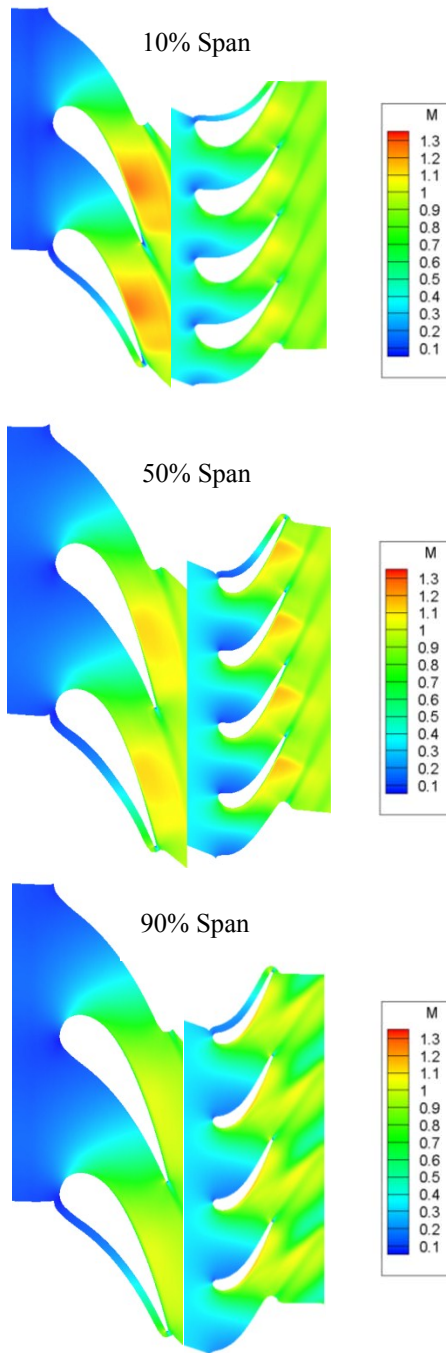


**Figure 5-1: Mach number contours of the stator and rotor blades at different span wise locations**

## 5.2. UNSTEADY SIMULATION

The simulations are run at the rotational speed of 9500 rpm with the same boundary conditions as the steady simulations. The time step size is determined individually for each case regarding number of rotor blades and the rotational speed. The convergence assumed to be established by a difference of less than 0.1% between two

successive peaks of the unsteady tangential force on the rotor blade. Figure 5-2 shows the unsteady tangential force measured on the rotor blade of S3R7 case.

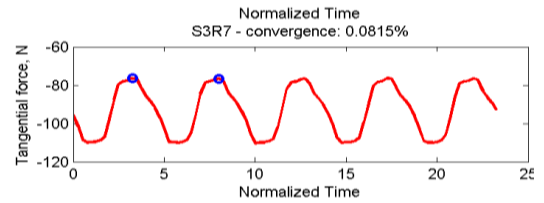


**Figure 5-2: Unsteady tangential force monitoring for convergence check, rotor, S3R7**

## SPACE-TIME PLOTS

The unsteady pressure distribution on a blade section can be depicted over time through the so called *space-time plots*. It enables the detailed study of the unsteady excitation sources, excited chord wise locations, their phase difference and amplitude. Time is normalized by the time of one passing stator. The chord wise location is normalized by the rotor mid-span chord, and the normalized unsteady pressure is extracted through equation (12). Figure 5-3 where depicts such plots for the rotor blade of S8R15 at 90% span. The nature of unsteadiness will be discussed in the following chapters.

$$\tilde{p} = \frac{p - \bar{p}}{p_0} \quad (12)$$

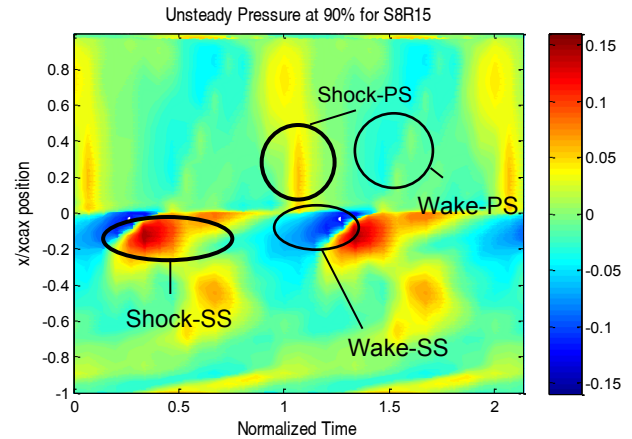


**Figure 5-3: Space-time plot of the rotor blade at 90% span**

To verify the steady aerodynamic viability of scaled cases, the normalized time averaged pressure at 10%, 50%, and 90% of span is depicted in Figure 5-4. The averaged pressure is consistent throughout the scaled stator blades. The same condition persists for the rotor blade except at 90% of span. Disagreements can be located in that region near the leading edge which experiences the effects from interacting shock waves formed on the stator blade. In addition, the provision for tip clearance augments the shock effects acting in that region in contrast to other span wise locations. It can be observed that S3R5 that retains the highest stator modification also shows slightly higher discrepancies in that region.

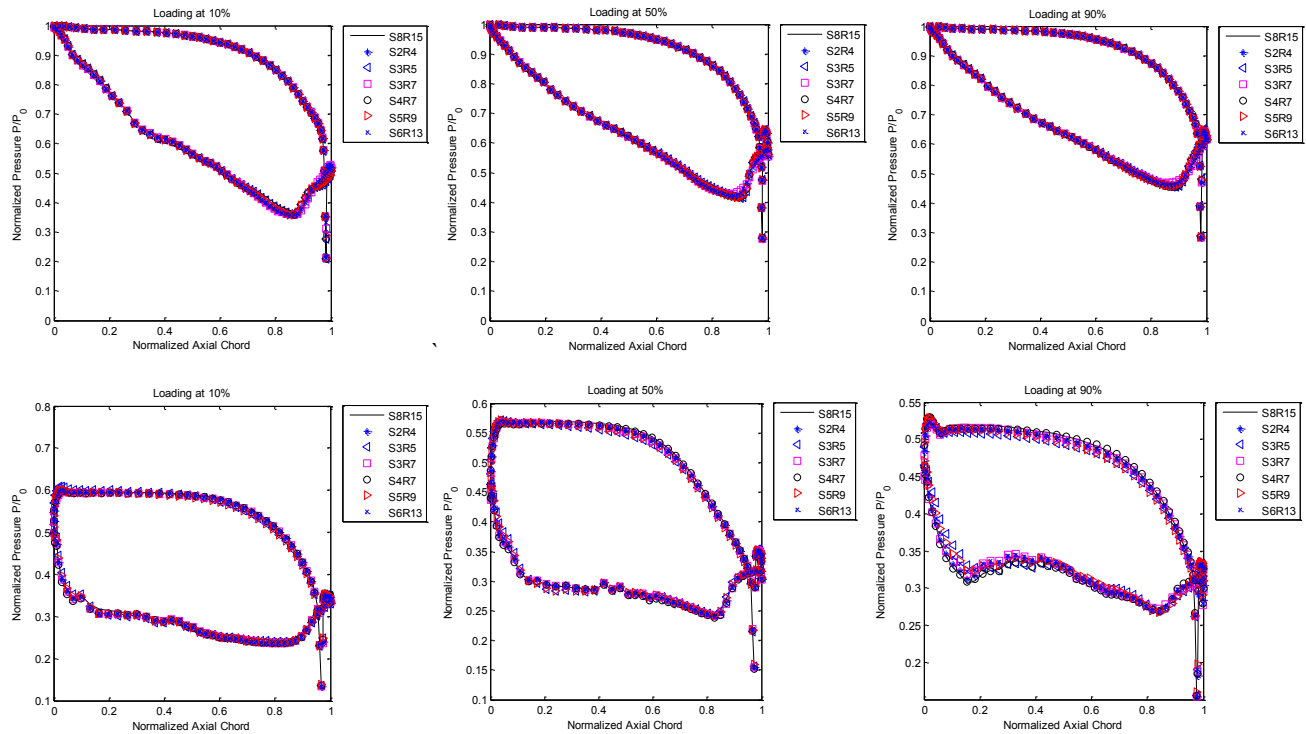


Figure 5-4: Time averaged unsteady pressure at span wise location for stator blades (top) and rotor blades (bottom)

### 5.3. STATOR GENERALIZED FORCES

As noted above the accuracy of this method is investigated through its capability in predicting generalized forces. Figure 5-5 depicts the predicted generalized forces on the stator blade for 60<sup>th</sup> EO (1<sup>st</sup> Harmonics) along 20 modeshapes. The response level is expected to lie in a low level since it roots in the downstream potential fields. In most cases over prediction of the generalized forces can be observed mainly for very high values of the scaling ratio. Nevertheless for slight changes of geometry the most risky modes are captured. It is coherent with the primary desired application of this technique for iterative design processes.

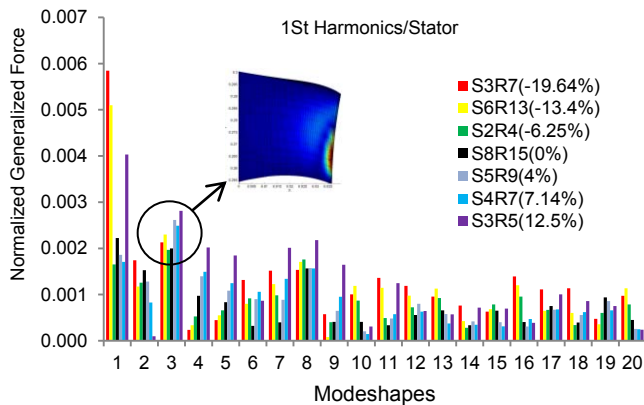
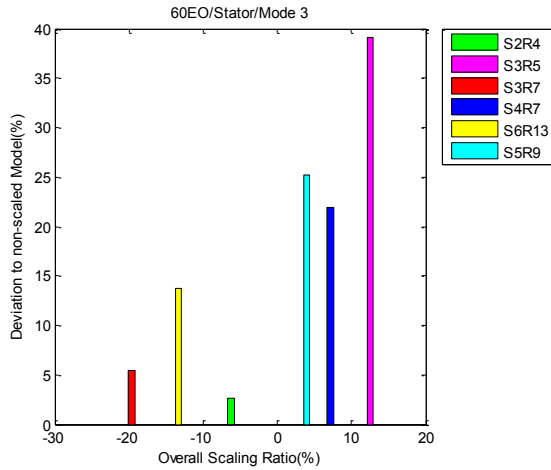


Figure 5-5: Normalized generalized forces for 20 modeshapes, 60<sup>th</sup> EO

The existence of resonance is riskier for lower modeshapes, regarding the operating envelope of most conventional turbomachines, and the energy of oscillation carried by such resonance occurrences is considerable. Accordingly the 3<sup>rd</sup> mode is selected which has a relative high generalized force response, to validate the accuracy of this technique. Figure 5-6 shows the absolute error of each scaled case versus the overall scaling ratio. There is a clear-cut distinction between the positive and negative values of overall scaling ratios. The positive scaling ratios show very large deviations as a result of geometrical modification of the stator blade. On the other hand the negative scaling ratios display a negligible sensitivity towards geometrical modifications in this specific modeshape. The most accurate prediction belongs to S2R4 with -6% of overall scaling ratio. Further negatively scaled configurations also show good agreement with the non-scaled configuration. It must be noted that mode 1 also shows relatively high generalized force response level and the absolute error for highly scaled cases are direr.

The RMS (Root Mean Square) values for 20 modeshapes are presented in Figure 5-7 in order to obtain an overall picture of the accuracy of this technique in predicting further modeshapes of the stator blade. In contrast to the previous comparison of the generalized forces of mode 3, similar trends are observed for both positively and negatively scaled cases. Additionally RMS values grow monotonically with increments in the absolute overall scaling ratio. The order of magnitude is nearly one order

lower than the predicted generalized forces for absolute overall scaling ration lower than 10.



**Figure 5-6: Deviation to non-scaled model for stator Mode 3, 60<sup>th</sup> EO**

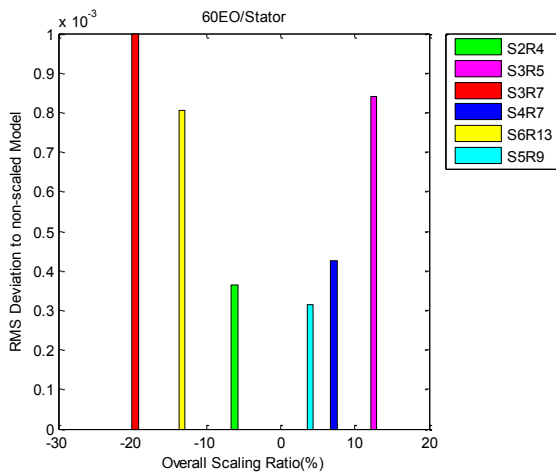


**Figure 5-7: RMS deviation to non-scaled model, stator 60<sup>th</sup> EO**

## DISCUSSION

In this section a more detailed analysis is performed on the results to clarify the physics of the contributing errors. The large existing errors in predicted generalized forces are mainly due to the heavy dependence of flow features on the geometry, and the different steps in calculation of generalized forces; in addition, the value of generalized forces is very small which can match the uncertainty level of simulations.

Different blade numbers in a row change the frequency of excitations for the neighboring blade row. Such perturbations are discrete which makes them highly frequency dependent. In spite of the frequency correction the contributing errors remain considerable. Furthermore the potential field on the rotor blade is subjected to continuous impact from the propagating shockwaves and wakes formed by the stator blades. Regarding the presented results such interactions between shockwaves, wakes and potential fields

of the stator and rotor blades prove to be heavily dependent on geometrical modifications. For instance, in Figure 5-5, S3R7 (-19.6%), and S4R7 (7%) both have the same excitation frequency; nevertheless S3R7 where the stator blade is subjected to lower modifications shows better accuracy in this particular modeshape. On the other hand it was observed in the previous section that the average RMS values behave similarly for the positively and negatively scaled cases. This indicates variable effects from frequency change, interacting shockwaves and wakes for each individual modeshape.

Furthermore, Figure 5-8 shows the harmonic forces acting on the stator blade of S8R15 (non-scaled) and back-scaled S3R7 (-19%). It is apparent how extreme scaling ratios can significantly change the magnitude and phase of oscillations.

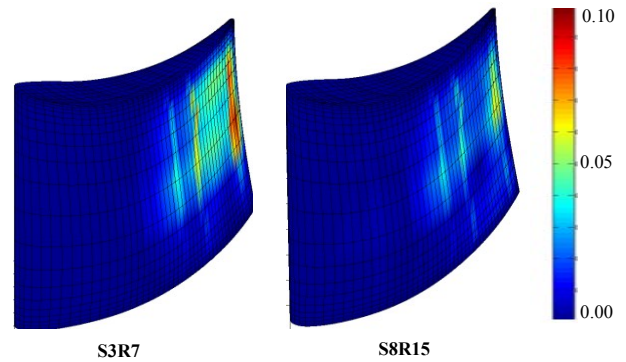


**Figure 5-8: Amplitude of the 1<sup>st</sup> harmonic forces on the suction side of stator, back-scaled S3R7 (left), S8R15 (right)**

In each scaled configuration the extent of influenced regions on the suction side near the trailing edge varies remarkably. Accordingly the generalized forces are a result of the dot product of the harmonic force vectors and the eigenvectors of the structure; thereby if the eigenvectors of the structure are large in that region such variations in the harmonic force vectors can result in larger errors. Figure 5-9 shows the eigenvectors of the 1<sup>st</sup> structural modeshapes. The concentration of large eigenvectors in the trailing edge, where excitation sources are dominant is apparent. The interpolation applied in mapping of FEM and CFD meshes also contributes to additional errors. The error contribution from the latter is trivial and dependent on the quality of the FEM and CFD meshes.

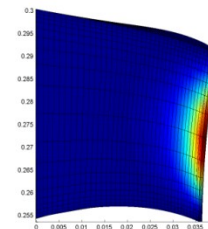


**Figure 5-9: Displacement of Stator 1<sup>st</sup> structural modeshape**

## 5.4. ROTOR GENERALIZED FORCES

Figure 5-10 illustrates the normalized generalized forces along 20 modeshapes of the rotor blade for 32<sup>nd</sup> EO (1<sup>st</sup> harmonics). A qualitative comparison indicates that higher errors exist for lower modeshapes. On the other hand smaller deviations are observed for higher modeshapes. The generalized forces are one order higher than the stator ones. It emphasizes the stronger influence from the upstream perturbations, namely, wakes and shockwaves.

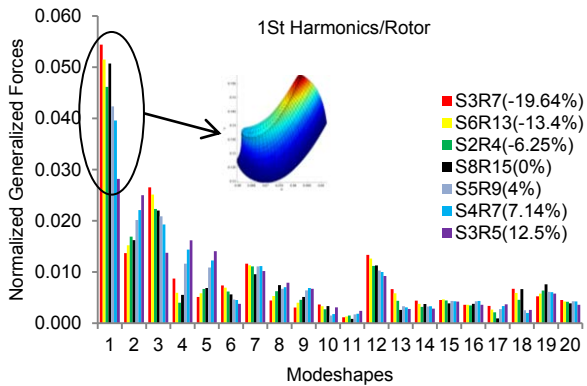


**Figure 5-10: Normalized generalized forces for 20 modeshapes, 32<sup>nd</sup> EO**

Similar to the stator most risky modes are located among the first modeshapes; thereby the ability of this method to well predict the response of these modes is a decisive factor. Figure 5-11 illustrates the deviation of the predicted generalized forces of the scaled cases to the non-scaled configuration for the 1<sup>st</sup> modeshape of the rotor blade. It is apparent that deviations are more sensitive to positive scaling values where the stator blade is exposed to relatively greater modifications through contraction. The average absolute error level is also higher for positively scaled cases. For instance, case S3R7, where the rotor blade alone is contracted to 15%, of its size, the error is far smaller than for S3R5, where the stator blade is shrunk merely 6% in size. The minimum error for this mode belongs to S6R13 with -13% overall scaling ratio where the stator blades are expanded by 6.6% and the rotor blades are contracted by 8%.

Figure 5-12 illustrates the RMS deviations of the scaled cases with respect to the non-scaled geometry. It can be reaffirmed that the negative overall scaling ratios fall within a smaller deviation margin than positive ones. On the other hand the positive scaling ratios show higher sensitivity with geometrical modifications. Moreover it can be concluded that the errors rise monotonically with increments in absolute overall scaling ratio. The increment rate of positive scaling values however is double its negative ones. Additionally it must be noted that the average RMS value of the scaled rotor blades is one order of magnitude higher than the scaled stator blades.

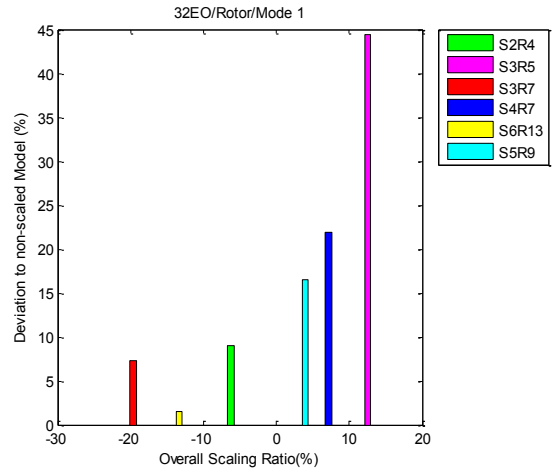


**Figure 5-11: Deviation to non-scaled model for rotor Mode 1, 32<sup>nd</sup> EO**

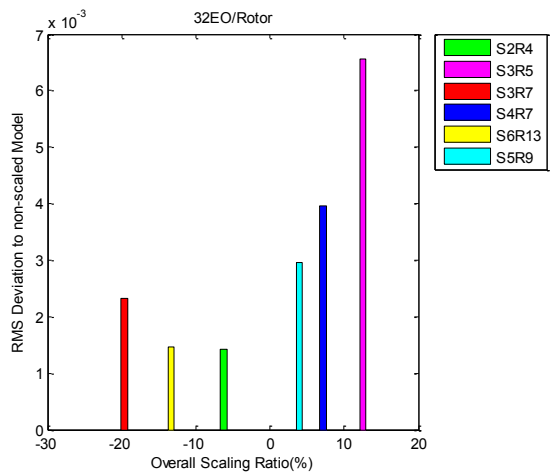


**Figure 5-12: RMS deviation to non-scaled model, rotor 32<sup>nd</sup> EO**

In addition, the 2<sup>nd</sup> harmonic forces can have considerable forced response levels once originated by upstream perturbations. As such the generalized forces for 64<sup>th</sup> EO are illustrated in Figure 5-13. A qualitative comparison reveals the massive discrepancies in the first couple of modeshapes (1-5). A number of drastic over and under prediction is discernable particularly for cases with a high excitability level.

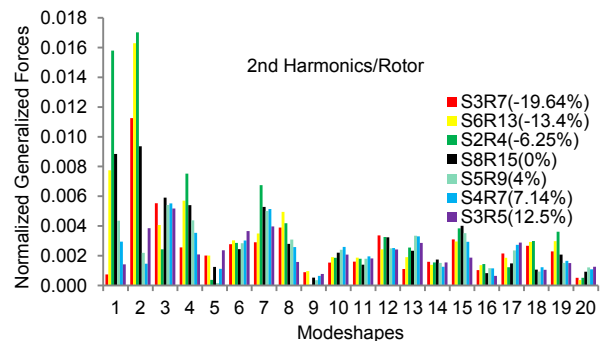


**Figure 5-13: Normalized generalized forces for 20 modeshapes, 64<sup>th</sup> EO**

The RMS deviation for 20 modeshapes for 64 EO is calculated to quantify the aforementioned, (see Figure 5-14). The difference between the RMS value of different scaled cases amounts to less than 0.1%; thereby no major relationship can be identified among the scaled cases. In contrast to the 1<sup>st</sup> harmonics, the RMS values seem somewhat insensitive towards geometrical modifications. It can be inferred that the scaling technique gives result with high deviations from the non-scaled configuration in the case of the 2<sup>nd</sup> harmonic forces, particularly for lower modeshapes.

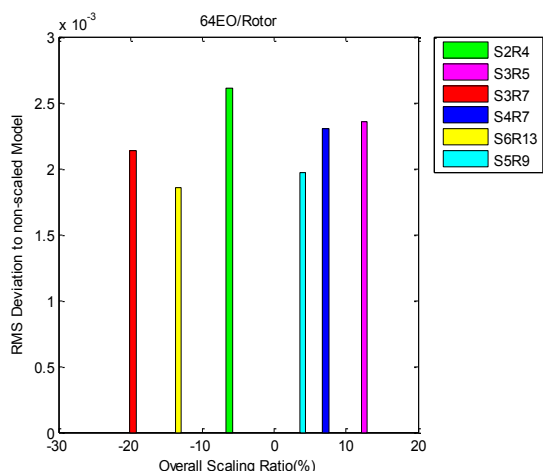


Figure 5-14: RMS deviation to non-scaled model, stator 64<sup>th</sup> EO

**DISCUSSION**

Figure 5-15 shows the absolute harmonic force amplitude on the rotor blade of S8R15 (non-scaled), and S3R5 (12.5%). Different regions on the rotor blade are affected with distinguishable difference in forcing amplitude, and phase. This can be explained through the nature of the prevalent upstream unsteadiness, i.e. shock waves and wakes. Moreover their potential interactions with each other and potential fields create a complex flow feature strengthening their dependency on geometry. Scaling also changes the trailing edge thickness the interblade row gap. The variation of the latter is within -3% to 3.5% of rotor blade chord. Consequently the wake strength and thickness greatly change which influences the extent of affected regions on the rotor blade. For instance S3R5, where the stator blade is shrunk, the unsteadiness has influenced a broader area on the leading edge of the rotor blade. Similarly, shockwaves significantly change in angle and strength causing considerable amplitude and phase change between scaled cases; in addition the gap change can additionally change the shockwave excited regions on the rotor blades.

How such differences in phase and amplitude influence the predicted generalized forces strongly depends on the individual modeshapes of the blade. The energy of oscillations are mostly carried by the first few modeshapes resulting in large eigenvectors; consequently higher

modeshapes possess lower energy and smaller eigenvectors result in smaller deviations once multiplied by the unsteady force vectors from different scaled configurations.

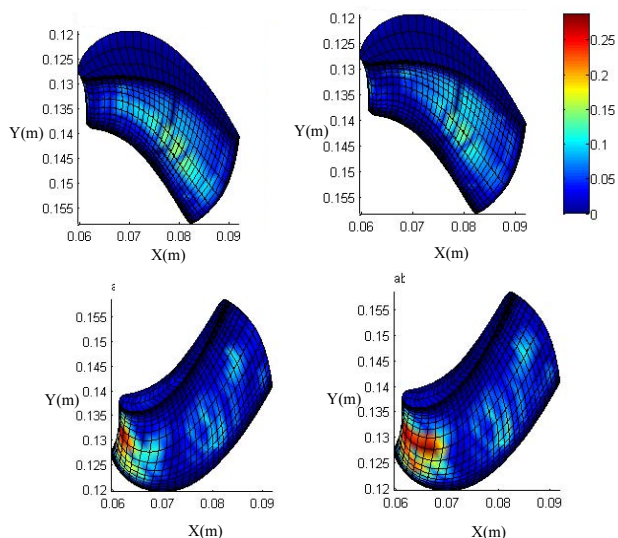


Figure 5-15: Amplitude of the 1<sup>st</sup> harmonic harmonic forces on the rotor blade S8R15 (left), S3R5 (right)

Figure 5-16 shows the 16<sup>th</sup> and 18<sup>th</sup> modeshapes of the rotor blade. Larger eigenvectors in the region most influenced by the unsteady pressure is one characteristic of mode 18. On the other hand mode 16 has moderate eigenvectors respectively. It is expected that the 18<sup>th</sup> mode shows larger discrepancies with the non-scaled case. A comparison between the predicted generalized forces from Figure 5-10 proves as such.

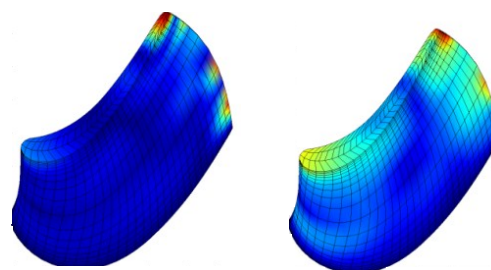
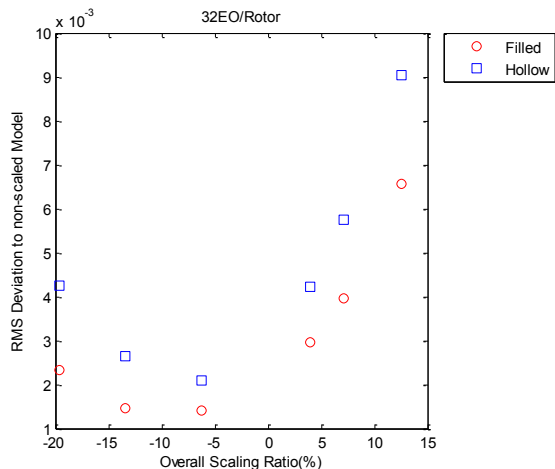


Figure 5-16: Displacement of the rotor blade 16<sup>th</sup> (left) and 18<sup>th</sup> (right) structural modeshape

Figure 5-17 shows the RMS values of different scaled cases along 20 modeshapes for two different structural models (EO 32). The additional structural model represents a hollow rotor blade with a shell thickness of 3mm; evidently, eigenvectors change between the two structural models. It is apparent that the hollow structural model for the rotor blade is less accurate than its counterpart. The latter proves high dependency of accuracy on the eigenvectors of structural model as well. In general since most turbine blades are treated with different cooling techniques the hollow model

is a more realistic representation of conventional turbine blades.



**Figure 5-17: RMS deviation to non-scaled model for filled and hollow structural model, Rotor 32<sup>nd</sup> EO**

In order to further clarify the relation between the flow features and the sources of error Figure 5-18 shows the space time plots for S8R15 at mid-span for two periods. As previously mentioned the time for one stator passing is assumed as one period. The phase line between two successive shock waves is also marked. It can be observed that the leading edge is subjected to strong pressure fluctuations. The pressure side and suction side are later influenced by weaker shock waves and diffused wakes.

The phase line of scaled and non-scaled is qualitatively drawn on the space time plot. The phase difference is distinguishable for different cases. It is interesting to note that the two cases with extreme scaling ratios, S3R7 (-19%) and S3R5 (13%) show the highest phase lag. These cases also proved to have the highest error calculated from RMS values for the 1<sup>st</sup> harmonics.

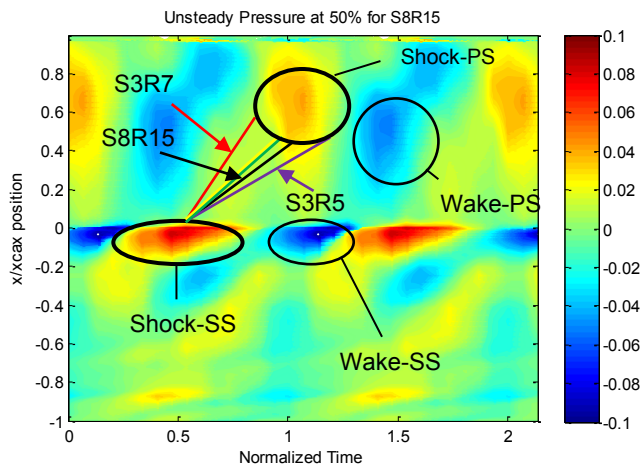


**Figure 5-18: Space-time plot of the rotor blade normalized unsteady pressure at mid-span, Phase line of non-scaled configuration and extremely scaled cases are marked.**

## 6. CONCLUSIONS

The effects of scaling on prediction of the generalized forces of a highly loaded transonic turbine stage have been studied. Results for 1<sup>st</sup> harmonic forces on the stator and rotor blade with additional 2<sup>nd</sup> harmonic forces on the rotor blade were presented for six scaled cases.

The generalized forces on the stator were presented for 20 modeshapes. High discrepancies were observed particularly for lower modeshapes; however cases where stator was exposed to none or slighter modifications showed better agreements for certain modeshapes and most risky modes were captured which can to some extent satisfy certain iterative design tools requirements. Moreover, the calculated root mean square (RMS) for 20 modeshapes proved monotonic proportionality with absolute overall scaling ratios.

Furthermore, results on the rotor blade showed better consistency for the 1<sup>st</sup> harmonics forces. The accuracy of results is driven by the amount of stator modification, in other words the upstream excitation sources showed substantial dependence on geometrical modifications. Alternatively negatively scaled cases proved better agreements both in RMS values and individual modeshapes. 2<sup>nd</sup> harmonics were also monitored for the rotor blade. Lower modeshapes showed high deviations and incoherent relations with the overall scaling ratio.

In conclusion scaling compromises accuracy proportional to the overall scaling ratio. Slight scaling ratios (5%) particularly towards negative scaling ratios can produce satisfactory results. Moreover the scaling technique can be a desirable tool for iterative design procedures if certain requirements such as minimum modification in upstream blade geometry in simpler flow regimes are met.

## ACKNOWLEDGEMENTS

This research has been funded by the Swedish Energy Agency, Siemens Industrial Turbomachinery AB, Volvo Aero Corporation, and the Royal Institute of Technology through the Swedish research program TURBOPOWER, the support of which is gratefully acknowledged.

## REFERENCES

- [1] Jöcker, M. 2002, "Mode Shape Sensitivity of the High Pressure Turbine Rotor Excitation due to Upstream Stators", ASME Paper No. GT-2002-30452
- [2] Vahdati M., Bread C., Simpson G., Imregun M., 2008. "Forced Response Assessment Using Modal Force Based Indicator Functions". Proceedings of ASME Turbo Expo 2008. GT2008-50306

- [3] Mårtensson, H., Forsman, J., Eriksson, M., 2009 “Simplified Forced Response HCF Assessment of Turbomachinery Blades”. ASME Paper No. GT2009-60166
- [4] Erdos, J. I., Alzner, E., 1977, “Numerical Solution of Periodic Transonic Flow through a Fan Stage”, AIAA Journal, 15, 1977, pp. 1559-1568
- [5] Giles, M. B., 1990, “Stator/Rotor Interaction in a Transonic Turbine”, AIAA Journal of Propulsion and Power, 6, 1990, pp. 621-627
- [6] Laumert B., Mårtensson H., Fransson, T.H., 2002, “Simulation of Rotor/Stator Interaction with a 4D Finite Volume Method”, ASME Paper No. GT-2002-30601
- [7] Clark, J.P., Stetson, G. M., Magge, S. S., Ni, R. H., Haldemann, C. W. and Dunn, M. G., 2000. “The Effect of Airfoil Scaling on the Predicted Unsteady Loading on the Blade of a 1 and ½ Stage Transonic Turbine and a Comparison with Experimental Results”, ASME Paper No. 2000-GT-0446
- [8] M. B. Schmitz, O. Schäfer J., Szwedowicz T., Secall-Wimmel, T. P. Sommer, 2006, “Axial Turbine Blade Vibrations Induced by the Stator Flow. Comparison of Calculations and Experiment”, Unsteady Aerodynamics, Aeroacoustics and Aerolasticity of Turbomachines, pp. 107-118
- [9] Mayorca, M.A, Jesús, D.A., Vogt, D.M., Mårtensson, H., Fransson, T., 2009, “Effect of Scaling of Blade Row Sectors on Prediction of Aerodynamic Forcing in a Highly-Loaded Transonic Compressor Stage”, ASME Paper No. GT2009-59601
- [10] Hilditch, M. A., Fowler, A., Jones, T. V., Chana, K. S., Oldfield, M. L. G., Ainsworth, R. W., Hogg, S. I., Anderson, S. J., and Smith, G.S., 1994, “Installation of a turbine stage in the Pyestock Isentropic Light Piston Facility”, ASME Paper No. 94-GT-277.
- [11] Hilditch, M. A., Smith, G.S. and Singh, U. K., 1998, “Unsteady flow in a single stage turbine”, ASME Paper No. 98-GT-531.